Calculated elastic constants and structural properties of Mo and $MoSi_2$

M. Alouani and R. C. Albers
Theoretical Division, Los Alamos National Laboratory, Los Alamos, New Mexico 87545

M. Methfessel
Fritz Haber Institut, Faradayweg 4-6, 1000 Berlin 33, Germany
(Received 29 August 1990; revised manuscript received 2 November 1990)

Using an all-electron, self-consistent, full potential, linear muffin-tin-orbitals method within the local-density approximation of density-functional theory, we have studied the structural properties and the elastic constants of Mo and $MoSi_2$. The Mo and $MoSi_2$ ground-state properties, lattice parameters, cohesive energy, and (for Mo) elastic constants are found to be in good agreement with the experimental results. Different structures in the angle-integrated photoemission spectrum of $MoSi_2$ can be satisfactorily explained in terms of various features present in the calculated total density of states. Since there have been no previous theoretical or experimental determinations, our calculations provide the first available information on the elastic constants of $MoSi_2$. For both Mo and $MoSi_2$ we have calculated the stress tensors for the experimental structures and have minimized their elastic energies. We have found that the lattice parameters and the ground-state total energies of Mo and $MoSi_2$ obtained from both the elastic energy and the total-energy minimizations are about the same, and that the lattice parameters are close to their experimental values.

I. INTRODUCTION

Transition-metal silicides (TMS) have important applications in the microelectronics industry. They can be used in integrated circuits for Schottky barriers, Ohmic contacts, and low-resistance gates and interconnections.[1] They are also, in general, chemically stable and resistant to corrosion. Some TMS have high electrical conductance;[2] others can be used as interface diffusion barriers.[3]

The low resistivity and the high-temperature stability of the silicides[2,4] has motivated many studies of their electronic and structural properties.[5–13] Spectroscopic techniques[5–7] have been used intensively to understand the nature of the chemical bonds in the TMS compounds. Several different local-density methods[6–13] have also been used to investigate the band structures of TMS, especially $MoSi_2$ and WSi_2. The latter have been studied in several papers by Kleinman and co-workers,[8–11] who used a full relativistic as well as a semirelativistic self-consistent norm-conserving pseudopotential approach. They focused mainly on the transition-metal-silicon and silicon-silicon chemical bonding. They also analyzed and compared the cohesive energy for $MoSi_2$ and WSi_2. The larger cohesive energy of WSi_2 relative to that of $MoSi_2$ was attributed to the more diffuse nature of the W $5d$ electrons, which allowed the formation of stronger covalent bonds. The electronic structure and the ground state of $MoSi_2$ have also been calculated by the linear muffin-tin-orbitals method in the atomic-sphere approximation (LMTO-ASA).[12,13] It was found that the spin-orbit coupling had little effect on its band structure and that the addition of an "Ewald correction" to the total energy improved the ground-state properties.

Besides its important microelectronics applications, $MoSi_2$ is also an important technological material because of its high-temperature (1000 °C – 1700 °C) ductility and oxidation resistance. This ductility means that components made from $MoSi_2$ will be much more reliable and significantly less susceptible to catastrophic fracture than structural ceramics, which are the only competitive materials in this temperature range. Potential applications include advanced furnace heating elements and high-temperature turbine blade components. Before this material can realize its true potential, however, two fundamental problems must be solved. First, its excellent oxidation resistance between 1000 °C–1700 °C breaks down with a completely destructive oxidation between 300 °C – 600 °C. This phenomenon has been called[14] the "$MoSi_2$ pest." Second, while $MoSi_2$ has excellent ductility at high temperatures, it is very brittle at room temperature; for ease of fabrication and for practicality it is very important to find ways to significantly lower the room-temperature brittle-to-ductile transition temperature. At a minimum, to develop new strategies for doing this requires understanding the basic mechanical properties of the pure single crystal.

Because it is difficult to grow single crystals large enough for elastic constant measurements, in this paper we have attempted a theoretical investigation of the ground state and the elastic constants of $MoSi_2$. In order to test our method, we have also studied the ground state and the elastic constants of Mo, since there are many experimental and theoretical results to compare with for

this material.[15–23]

Our local-density-approximation (LDA)[24] density-functional calculations used an all-electron, full-potential, linear muffin-tin-orbitals method (FP-LMTO), which was recently developed by one of us.[25] This method is fast and accurate, and has been successfully used to obtain the structural and dynamical properties of silicon,[26] as well as the structural properties of the first-row transition metals.[27]

The remainder of the paper is organized as follows: In Sec. II we introduce our method of calculation, in Sec. III we present and discuss our results, and Sec. IV contains our summary and conclusions.

II. METHOD OF CALCULATION

A. Total energy calculation

The standard LMTO method in the atomic-sphere approximation (ASA) uses Hankel functions with vanishing kinetic energy ($\kappa^2 = 0$) and neglects the nonspherical parts of the electron density.[28] It can only usually accurately describe isotropic deformations, such as hydrostatic-pressure variations of the total energy. Because a nonisotropic deformation is very sensitive to the nonspherical part of the charge density and the potential, as well as to systematic errors due to overlap of the atomic spheres, it is necessary to go beyond ASA and use a full-potential method to describe elastic properties, phonon displacements, or, for molecular-dynamics, density-functional calculations.

Many full-potential methods are now available, but, unfortunately, they are often very computationally expensive. If one starts from a "muffin-tin" geometry, where the space is divided into nonoverlapping atomic spheres and an interstitial region, then one can easily construct muffin-tin orbitals, which are Hankel functions outside the muffin-tin spheres and are augmented by the numerical solution of the Schrödinger wave function inside the muffin-tin spheres. Using this basis set, which was introduced by Andersen,[28] one of us[25] has recently developed a full-potential method which, for well-packed systems, is as accurate as existing full-potential methods, but at least 1–2 orders of magnitude faster. To calculate the total energy for any arbitrary strain we shall make use of this method. Inside the spheres, spherical harmonic components of the charge density are included explicitly for ℓ up to 4. The interstitial density is obtained by matching a linear combination of atom-centered Hankel functions with $\ell \leq 4$ and with two different kinetic energies to the values and slopes of the sphere densities. The "tails" with $\ell > 4$ of the Hankel functions extend into the spheres so that the final density is continuous and smooth, and includes angular momentum terms to infinite ℓ in the spheres. This representation of the charge density is very useful because Poisson's equation can be solved analytically for the interstitial region and by straightforward numerical integration inside the spheres. To evaluate the matrix elements of the interstitial potential, the product of two Hankel functions, which represent LMTO envelope functions, is fitted in the interstitial by a linear combination of Hankel functions in the same way as the charge density. More details about the method can be found elsewhere.[25]

In this calculation the full-potential LMTO (FP-LMTO) uses a triple-κ set with fixed κ values. The electronic structures of Mo and $MoSi_2$ are obtained using a two-energy-panel calculation; one panel is used to calculate the valence electrons and one to calculate the Mo $4p$ electron states, which extend beyond the Mo muffin-tin spheres. Thus, the Mo $4p$ electrons are treated as bands in the same way as the valence electrons. In diagonalizing the Hamiltonian for these "semicore" Mo $4p$ electrons we have used only an sp basis set and six special $\mathbf{k}$ points.[29] More $\mathbf{k}$ points shows no significant effect on the band structure or total energy. The core electrons are not treated in the frozen-core approximation, but are allowed to relax; the core-electron charge density is recalculated at each iteration in the self-consistency loop. The Von Barth and Hedin[30] exchange-correlation energy and potential were used and the relativistic effects were neglected. The Brillouin zone integration used a Gaussian sampling[31] with 30 equally spaced $\mathbf{k}$ points in the irreducible part of the tetragonal Brillouin zone (IBZ). When a strain is introduced in the crystal, the number of irreducible $\mathbf{k}$ points is recalculated for the symmetry of the distorted crystal. In all calculations of ground-state properties of Mo and $MoSi_2$ we have used fixed muffin-tin radii of 2.45 a.u. for Mo and 2.25 a.u. for Si.

The cohesive energy of $MoSi_2$ has also been calculated. The total energy for isolated Mo and Si atoms has been obtained by means of a spin-polarized LDA method. The electronic configuration corresponding to Hund's rule was found to give the minimal total energy.

The equation of state (pressure versus volume) of $MoSi_2$ and the bulk modulus for both Mo and $MoSi_2$ were calculated from a least-squares fit of the total energy as a function of unit-cell volume to the Birch-Murnaghan equation of state.

B. Elastic constants

The self-consistent first-principles FP-LMTO is used here to predict for the first time the elastic constants of $MoSi_2$. The stress tensor and the elastic constants can be defined in different ways and it is useful to define our notation. In the following we shall briefly list the relevant formulas needed to obtain the elastic constants of body-centered tetragonal $MoSi_2$ (crystal structure type $C11b$), which has a D_{4h}^{17} ($I4/mmm$) space group, and of body-centered-cubic Mo. We consider strains with and without volume conservation, because volume-conserving strains alone do not provide enough constraints to determine all six elastic constants of $MoSi_2$. We shall consider only small lattice distortions in order to remain within the elastic domain of the crystal.

After a uniform deformation of the solid, a Bravais-

lattice point that is at $\mathbf{R}$ in the undistorted lattice will be moved to $\mathbf{R}'$, such that

$$R_i' = \alpha_{ij} R_j \ , \tag{1}$$

where R_i and R_i' are the rectangular components of the lattice vectors $\mathbf{R}$ and $\mathbf{R}'$, respectively, $i = x$, y, or z, and where the matrix α is given by

$$\alpha_{ij} = \delta_{ij} + \epsilon_{ij} \ . \tag{2}$$

Note that we are using the Einstein summation convention in this paper, where repeated indices are to be summed over. The strain tensor $\mathbf{e}$ is defined to be

$$e_{ij} = \epsilon_{ij} + \epsilon_{ji}(1 - \delta_{ij}) \ . \tag{3}$$

The internal energy of a crystal under strain $\mathbf{e}$ can be expanded in powers of the strain tensor with respect to the initial internal energy $E(V)$ of the unstrained crystal:

$$E(V, \mathbf{e}) = E(V) + V\tau_{ij} e_{ij} + V C_{ijkl} e_{ij} e_{kl}/2 + \cdots \ , \tag{4}$$

where $\tau_{ij} = [(1/V)\partial E/\partial e_{ij}]_{e'}$ is the stress tensor, $C_{ijkl} = [(1/V)(\partial^2 E/\partial e_{ij}\partial e_{kl})]_{e'}$ are the second-order adiabatic elastic constants, and V is the volume of a unit cell before the crystal is strained. Here the subscript e' indicates that all other e_{mn} are kept constant while differentiating with respect to e_{ij} or e_{kl} . Using the symmetry properties of τ, C, and $\mathbf{e}$, and the standard notation $xx \equiv 1$, $yy \equiv 2$, $zz \equiv 3$, $yz \equiv 4$, $zx \equiv 5$, $yx \equiv 6$, we can rewrite Eq. (4) as[32]

$$E(V, \mathbf{e}) = E(V) + V\tau_i e_i + V C_{ij} e_i e_j/2 + \cdots \ , \tag{5}$$

where the summation indices now range from 1 to 6 instead of over x, y, and z. Note that the strain tensor τ is zero (the first derivative of the energy is zero), if the crystal is at equilibrium. In our calculations we always use the experimental geometry as the starting point for the elastic energy expansion. Because this is not usually identical with the structure that minimizes the total energy, we will typically have nonzero τ's present.

For a tetragonal crystal there are only six independent elastic constants: $C_{11} = C_{22}$, C_{33}, $C_{44} = C_{55}$, C_{66}, C_{12}, and $C_{13} = C_{23}$. All of the rest are either zero or follow from the general condition $C_{ij} = C_{ji}$. For the more symmetric cubic crystal there are only three nonzero independent elastic constants: $C_{11} = C_{22} = C_{33}$, $C_{12} = C_{13} = C_{23}$, and $C_{44} = C_{55} = C_{66}$.

In order to calculate the stress tensor τ_i and the elastic constants C_{ij}, we have calculated the local-density total energy as a function of different deformations of Mo and $MoSi_2$; we have used the experimental structures as the points of expansion. For small deformations the total energy can be fit to the expansion, Eq. (5), with the appropriate values of e_i for each specified deformation. For both $MoSi_2$ and Mo we have used enough independent distortions in order to determine the relevant strains and elastic constants. Note that the change of volume involved in each deformation is given by

$$(V - V_0)/V_0 = e_1 + e_2 + e_3 \ . \tag{6}$$

Pure shears are those deformations that have no volume change. Note also that a crystal under a uniform pressure p has a strain tensor given by $\tau_1 = \tau_2 = \tau_3 = -p$ and $\tau_4 = \tau_5 = \tau_6 = 0$.

Out of the many different possible choices we have found it convenient to use the following six independent deformations for $MoSi_2$ [cases (a)–(f)]:

$$\text{case (a)}: \ e_1 = -2e_2 = -2e_3 = \epsilon \ ,$$
$$\text{case (b)}: \ 2e_1 = 2e_2 = -e_3 = -\epsilon \ ,$$
$$\text{case (c)}: \ e_1 = e_2 = -e_3/2 = e_6/6 = \epsilon/4 \ ,$$
$$\text{case (d)}: \ e_1 = \epsilon \ ,$$
$$\text{case (e)}: \ e_3 = \epsilon \ ,$$
$$\text{case (f)}: \ e_4 = 2\epsilon \ .$$

In each case the other components of the strain tensor are equal to zero. For Mo, since there are only three independent elastic constants, we have used the following three independent deformations:

$$\text{case (a)}: \ 2e_1 = 2e_2 = -e_3 = \epsilon \ ,$$
$$\text{case (b)}: \ e_3 = \epsilon \ ,$$
$$\text{case (c)}: \ e_6 = 2\epsilon \ .$$

For each of the above cases we have used five different values of ϵ: $\epsilon = 0, \pm 0.02, \pm 0.04$. The difference in the internal energy in Eq. (5) is then fitted to polynomials of order 2, 3, and 4 for each case in order to extract a linear term in ϵ with a prefactor involving combinations of the τ_i and a squared term in ϵ with a prefactor involving combinations of the C_{ij}. To check the consistency of our results for $MoSi_2$ we have also used another shear strain $e_6 = 2\epsilon$, which allows C_{66} to be obtained separately. The bulk modulus (at fixed c/a) has also been used as an additional check, since $B = V\partial^2 E/\partial V^2 = (1/V)\partial^2 E/\partial\epsilon^2$, where $\epsilon = (V - V_0)/V_0$. For $MoSi_2$ we then find

$$B = \tfrac{2}{9}(C_{11} + C_{12} + 2C_{13} + C_{33}/2) \ , \tag{7}$$

and for Mo

$$B = \tfrac{1}{3}(C_{11} + 2C_{12}) \ . \tag{8}$$

In the case of $MoSi_2$, the calculation of τ also includes the strains obtained from cases (a), (d), and (f) by exchanging the x and y directions. Thus, we obtain a system of ten linear equations for τ and seven linear equations for C_{ij}. Since these systems of linear equations are overdetermined, we have solved them by using a linear least-squares algorithm based on a singular-value decomposition technique. For Mo, we have also included the strains obtained by interchanging x, y, and z. This led to nine different linear equations for the stress tensor. This procedure guarantees that the stress tensors of Mo and $MoSi_2$ have their correct cubic ($\tau_1 = \tau_2 = \tau_3$, $\tau_4 = \tau_5 = \tau_6$) and tetragonal ($\tau_1 = \tau_2$, $\tau_4 = \tau_5$) symmetries; it also considerably reduces the numerical noise in the determination of τ.

III. RESULTS AND DISCUSSION

A. Mo

Various theoretical methods[15–22] have been used to study the structural properties of Mo. In Table I we have listed results obtained with the Korringa-Kohn-Rostoker (KKR) method,[15] the nonlocal pseudopotential (NL-PP) method,[16] the linear combination of atomic orbitals (LCAO) method,[17] the pseudopotential linear combination of atomic orbitals (PP-LCAO) method,[19] the general potential linear augmented-plane wave (LAPW) method,[21] the full relativistic norm-conserving pseudopotential (NC-PP) method,[11] and the LMTO-ASA.[13,22,23] The results of our calculations for the structural properties of bulk Mo are also displayed in Table I. The total energy data are shown in Fig. 1. The solid line is a least-squares fit to the Birch-Murnaghan equation of state,[33] which has the form

$$E(V) = \sum_{n=1}^{4} a_n V^{-(2/3)(n-2)} . \quad (9)$$

Our fit to Mo is $a_1 = 0.224\,39\times10^4$, $a_2 = -0.104\,74\times10^6$, $a_3 = 0.129\,89\times10^7$, and $a_4 = -0.177\,72\times10^7$; this gives $E(V)$ in mRy/(unit cell) when V is in a.u.^{3}/(unit cell).

The cohesive energy may be determined by subtracting the atomic total energies from the solid-state total energy. We have used the same exchange-correlation energy of Von Barth and Hedin[30] for both the solid and the atomic calculations. The minimum of the total energy for the Mo free atom (in the $4d^5 5s^1$ electronic configuration) was found to be $E_{\rm Mo} = -7946.0891$ Ry. Our calculated cohesive energy for Mo of 6.862 eV is in fairly good agreement with the experimental value[34] of 6.82 eV. This is unusually good, because the LDA predicts an excess binding of about 1 eV per atom for most systems. We have checked that our bulk total energy changes by less than 0.05 eV if the basis is increased, more **k** points are used for valence and semicore panels, and the Gaussian broadening is reduced. A factor influencing the unexpectedly good agreement with the experimental cohesive energy is that cancellation of energy terms is significant, because a large spin-polarization contribution (−6.85 eV) enters into the free-atom energy. An important difference between our calculation and the general-potential LAPW calculation[21] is their use of the scalar-relativistic approximation, whereas our calculations were nonrelativistic. We have therefore done an additional scalar-relativistic calculation, which gave $E_{\rm coh}$=7.39 eV, which is in better agreement with the LAPW results. The remaining discrepancy of 0.39 eV could be due to a more approximate treatment of the semicore states used in the LAPW calculations.[21] For Mo, we have found that the total energy depends quite sensitively on the treatment of the $4p$ semicore states. In our calculations these states are treated accurately as band states. We point out that previous nonrelativistic calculations using the KKR method[15] and the LMTO-ASA method with nonspherical terms included and the $4p$ semicore states also treated as band states,[23] have obtained values of 6.732 and 6.880 eV, respectively, for the cohesive energy.

The calculated lattice parameter a and bulk modulus B_0 compare favorably with experiment,[35] the corresponding discrepancies being 0.3% and 3%, respectively. All the methods listed in Table I seem to accurately describe these quantities for Mo. In order to estimate the error bars on the lattice parameter and the bulk modulus, we have compared the results obtained by using n = 3, 4, and 5 in Eq. (9). This gives a=5.961, 5.982, and 5.970 a.u. and B_0= 2.512, 2.554, and 2.571 Mbar. The lattice constant and the bulk modulus are then obtained by averaging these values; the upper and lower bounds are obtained by averaging the absolute values

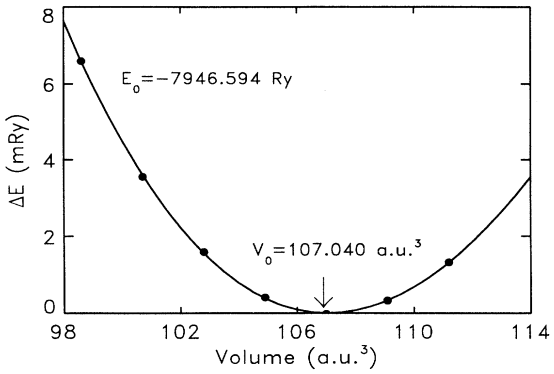

FIG. 1. Total energy of bcc Mo vs volume per unit cell. The total energy at equilibrium was chosen as the zero of energy. The solid curve is a least-squares fit to a Birch-Murnaghan equation of state (see text).

TABLE I. Calculated structural properties of bcc Mo compared to some experimental and theoretical results. The bulk modulus B_0 was obtained by taking the derivative of a third-order polynomial least-squares fit to the total energy as a function of volume.

	a (a.u.)	B_0 (Mbar)	$E_{\rm coh}$ (eV/atom)
Expt.	5.949[a]	2.608[a]	6.82[b]
KKR[c]	5.89	2.51	6.732
NL-PP[d]	5.956	3.05	6.678
LCAO[e]	5.99	2.57	6.28
PP-LCAO[f]	5.841	2.78	7.14
LAPW[g]	5.917	2.91	7.782
NC-PP[h]	5.858	2.705	7.782
Corr. ASA[i]	5.86	2.92	
LMTO-ASA[j]	5.977	2.753	
LMTO-ASA[k]			6.880
Present work	5.97±0.01	2.55±0.02	6.862

[a] Reference 35.
[b] Reference 34.
[c] Reference 15.
[d] Reference 16.
[e] Reference 17.
[f] Reference 19.
[g] Reference 21.
[h] Reference 11.
[i] Reference 13.
[j] Reference 22.
[k] Reference 23.

of the deviations from the main values. We then find $a = 5.97 \pm 0.01$ a.u. and $B_0 = 2.55 \pm 0.02$ Mbar. For all the other moduli we have used this same type of analysis to determine the numerical noise. For the stress tensor and the elastic constants polynomials of different orders are used for the least-squares fit as mentioned in the method of calculation.

Contour plots of the self-consistent valence charge density of Mo in the (001) and (110) plane are shown in Fig. 2. There is a formation of metallic bonds between the nearest-neighbor atoms with a minimum in the charge density between 50 and 60 millielectrons/a.u.^{3} and about 40 millielectrons/a.u.^{3} between the second neighbors. The total charge density seems to be spherical near the atomic sites.

Before attempting elastic constant calculations for $MoSi_2$, for which there is no experimental data, we have tested our method on Mo. Using the method described in Sec. II, we have obtained the three elastic constants of bcc Mo. The results are presented in Table II together with the previous Ewald-corrected LMTO-ASA calculation,[13] which includes "muffin-tin" corrections, and the experimental results.[36] As can be seen from Table II, our results are in good agreement with the experimental results, the discrepancies being 2%, 6%, and 11% for C_{11}, C_{12}, and C_{44}, respectively. The larger discrepancy for C_{44} may be because it involves a complicated distortion of the lattice. The Ewald-corrected LMTO-ASA gets C_{11} and C_{12} within 24% and 13%, respectively, of the corresponding experimental values. However, no value is given for C_{44} in Ref. 13, so it is not clear whether the success of the corrected ASA approach is valid more generally. We have also calculated the stress tensor and found that $\tau_1 = \tau_2 = \tau_3 = -0.40 \pm 0.01$ mRy/(a.u.)^3 and $\tau_4 = \tau_5 = \tau_6 = 0$ mRy/(a.u.)^3. This stress tensor will be used later for the minimization of the elastic energy of Mo.

TABLE II. Calculated elastic constants of bcc Mo in units of 10^{12} dyn/cm^2 compared to the experimental results of Ref. 36 and the Ewald-corrected LMTO-ASA calculation of Ref. 13.

	C_{11}	C_{12}	C_{44}
Expt.	4.50	1.729	1.25
Corr. ASA	5.6	1.51	
Present work	4.40±0.03	1.62±0.02	1.39±0.02

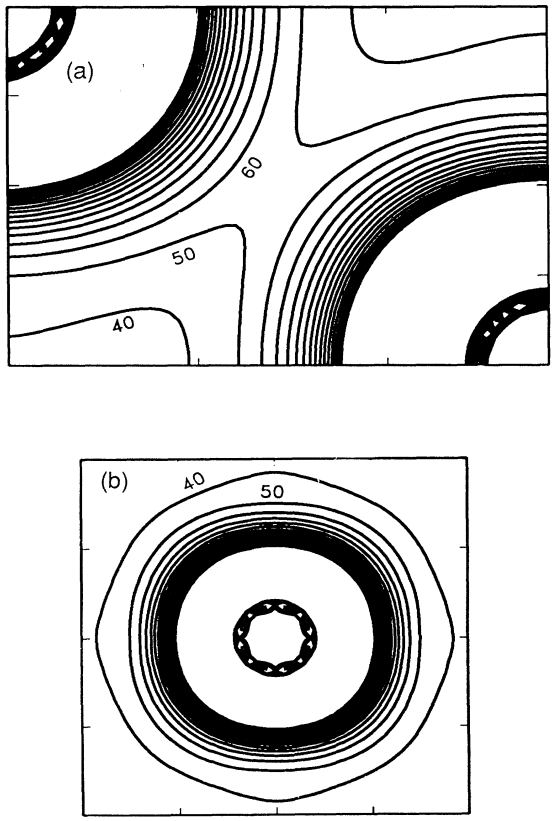

FIG. 2. Contour plots of constant charge density of Mo: (a) (001) plane, (b) (110) plane, in steps of 10 millielectrons per cubic bohr. Only the bonding regions of the charge density contours are labeled. The steps between the inner contours are also 10 millielectrons per cubic bohr.

In order to understand qualitatively why C_{11} is always larger than C_{44} for a cubic crystal, one can use the following argument: If one distorts the crystal in such a way that only C_{44} is involved, all the e_i's are zero except, for example, $e_4 = \epsilon$. Then the bond lengths between a Mo atom and its nearest neighbors in the (110) plane are stretched by $\epsilon a/(2\sqrt{3})$ and those in the $(1\bar{1}0)$ compressed by the same amount and vice versa if ϵ is negative (a is the lattice parameter). The second neighbors are all stretched by $\epsilon^2 a/8$. If one distorts the crystal so that only C_{11} is involved, then all the e_i's are zero except, for example, $e_1 = \epsilon$. The first neighbors will be all stretched or compressed by $\epsilon a/(2\sqrt{3})$ and the second neighbors along the [100] direction will all be stretched or compressed by ϵa. It is then obvious that the charge density in the latter case will be more distorted along the bonds than in the former case and consequently the total energy will increase much more in the latter case than in the former. Since the elastic constants are defined to be the second derivative of the total energy with respect to the strain, it is then clear that C_{11} is much larger than C_{44}.

B. $MoSi_2$

The total density of states (DOS) and the partial DOS for Mo and Si (obtained from a Gaussian sampling with a Gaussian smearing of 0.34 eV), which are shown in Fig. 3, are in good agreement with the calculation of Bhattacharyya, Bylander, and Kleinman.[10] The total DOS also compare well with the angle-integrated photoemission data of Weaver, Moruzzi, and Schmidt (WMS).[5] Thus, the strong peak with a 5-eV width observed by WMS at approximately 2 eV below the Fermi level can

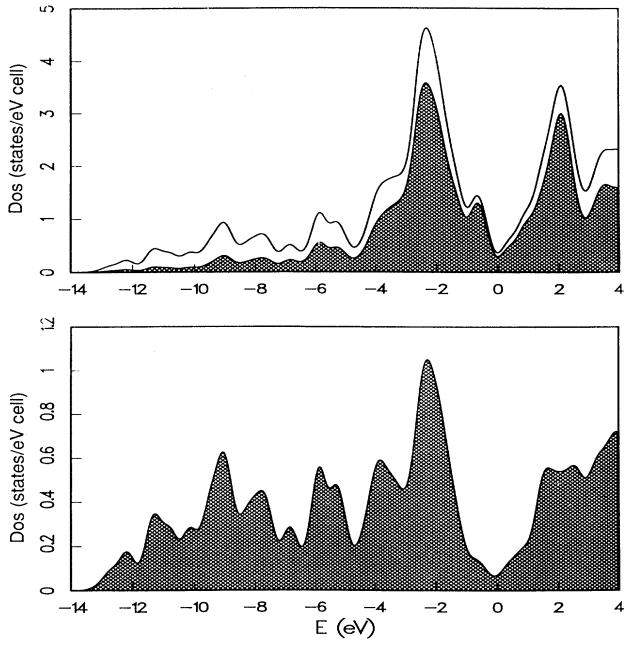

FIG. 3. Total and projected density of states (DOS) for Mo and Si in units of states per eV per unit cell. The Fermi level is at the zero of energy. The total DOS is the upper curve of the upper figure. The shaded area of the upper figure is the Mo contribution to the total DOS and the lower figure is the Si contribution.

be explained as being due mainly to the Mo $4d$ states with a very small Si $3p$ contribution, whereas the shoulder observed near 6 eV below E_F is explained in terms of our peak at 6 eV, which is a mixture of Mo $4d$ and Si $3p$ hybridized bands. The structures observed near 8 and 12 eV below E_F are mainly Si $3s$ states. The Fermi level falls in a deep minimum of the DOS, separating the bonding and the antibonding bands. This "quasigap" of the DOS near E_F indicates that there is a strong covalent contribution to the bonding and that the crystalline structure is very stable.

The results of our calculations for the structural properties of $MoSi_2$ are displayed in Table III together with

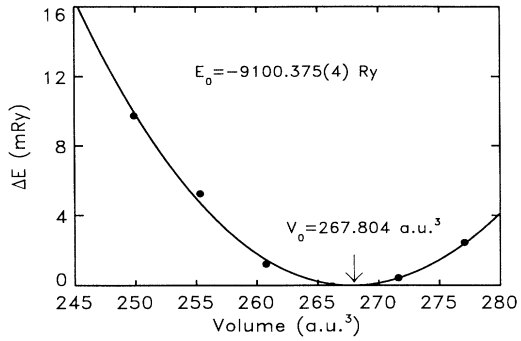

FIG. 4. Total energy of tetragonal $MoSi_2$ vs volume per unit cell. The total energy at equilibrium was chosen as the zero of energy. The solid curve is a least-squares fit to a Birch-Murnaghan equation of state (see text).

the available theoretical[11,13] and experimental results.[37] In these calculations we have first fixed a at the experimental value of 6.05 a.u. and then have varied c. The minimum-energy structure was found for $c = 14.80 \pm 0.01$ a.u. and hence a theoretical value for $c/a = 2.446$; this ratio compares favorably with the experimental ratio of 2.456. We then calculated the total energy as a function of volume with the ratio c/a kept equal to its theoretical value. This curve is presented in Fig. 4 with the equilibrium total energy taken to be the zero of energy. The solid curve in the figure is a least-squares fit to a three-term Birch-Murnaghan equation of state[33] with the fitted parameters: $a_1 = 0.112\,52 \times 10^3$, $a_2 = -0.935\,10 \times 10^4$, and $a_3 = 0.194\,23 \times 10^6$; this gives $E(V)$ in mRy/(unit cell) when V is in a.u.^{3}/(unit cell). The minimum of the total-energy occurs at $a = 6.02 \pm 0.01$ a.u., which is in good agreement (0.5% deviation) with the 6.05-a.u. experimental value. The parameter c was found to be 14.74 ± 0.01 a.u., which is about 0.8% lower than the experimental value.[38] The theoretical volume per unit cell is thus 2% smaller than the experimental volume. We have determined the bulk modulus by a least-squares fit of the total energy to polynomials of order 2, 3, and 4 in the volume; we obtained a value of 2.22 ± 0.03

TABLE III. Calculated structural properties of body-centered tetragonal $MoSi_2$ compared to the existing experimental and theoretical results. The bulk modulus B_0 was obtained by taking the derivative of a third-order polynomial least-squares fit to the total energy as a function of volume.

	a (a.u)	c (a.u)	B_0 (Mbar)	E_{coh} (eV/molecule)	H_f (eV/molecule)
Expt.	6.050[a]	14.858[a]		16.90[b]	1.36[c]
NC-PP[d]				19.694	1.78
Corr. ASA[e]	6.027	14.779	2.38		
Present work	6.02±0.01	14.74±0.01	2.22±0.03	19.148	1.87

[a]Reference 38.
[b]Reference 39.
[c]Reference 36.
[d]Reference 11.
[e]Reference 13.

Mbar. The bulk modulus that was obtained by a least-squares fit to a Birch-Murnaghan equation of state was 2.27 ± 0.03 Mbar, which is 0.05 Mbar higher. We anticipate that the former value is more accurate and consistent with the calculation of the elastic constants of $MoSi_2$ than the latter. Indeed, the bulk modulus obtained from Eq. (7) and our values for the elastic constants (see below) give a value of 2.06 ± 0.04 Mbar, which is closer to the polynomial-method value. The experimental bulk modulus is unknown, so our calculated value remains a prediction. Nevertheless our bulk modulus is comparable with the Ewald-corrected LMTO-ASA result, which is shown in Table III.

The cohesive energy of $MoSi_2$ compares favorably with the experimental value,[39] the discrepancy being about 9.8%. Our calculated cohesive energy differs from the NC-PP calculation by less than 3%. Using our calculated cohesive energy for Mo and that for Si obtained by Methfessel, Rodriguez, and Andersen,[26] we have calculated the heat of formation H_f of $MoSi_2$. Our calculated H_f was 0.51 eV higher than the experimental value,[37] but only 0.09 eV higher than the NC-PP value.[11] The discrepancy with experiment is probably caused by the error in evaluating the cohesive energies, which involves the subtraction of large numbers calculated by different methods.

We have also calculated the equation of state (the pressure versus volume) by taking the volume derivative of the fitted total energy; the result is shown in Fig. 5. Since there is no experimental or calculated equation of state for $MoSi_2$, our calculation should be a helpful point of reference for experimentalists.

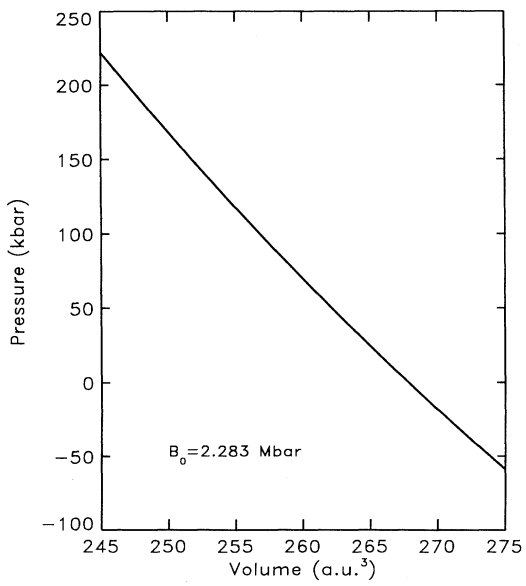

FIG. 5. Calculated pressure vs unit cell volume for tetragonal $MoSi_2$ with the c/a ratio fixed at the theoretical value. This curve was obtained by taking the first derivative (with respect to unit cell volume) of the Birch-Murnaghan equation state (see text).

The charge-density contours of $MoSi_2$ in the (001), (100), and (110) planes are depicted in Fig. 6. A three-dimensional plot of the charge density in the (100) plane is also shown in Fig. 7. Our calculated charge density is in good agreement with that calculated by Bhattacharyya, Bylander, and Kleinman,[8] who used the NC-PP method, except that ours is almost spherical around the Mo atoms (see, e.g., Fig. 7). There are eight Si nearest neighbors of Mo at a distance of 4.94 a.u. away, which lie in two square arrays, which are centered above and below the Mo atoms. The two Si second-neighbor atoms (along the z axis), just above and below the Mo atom, are located almost at the same distance from Mo (4.95 a.u. away). As shown in Fig. 6, the charge density seems to have a local axis of symmetry of order 6 perpendicular to the (110) plane. The bonds between Mo and the ten Si nearest neighbors have almost the same strength. The Si atom has four Si nearest neighbors 4.94 a.u. away in a square array, which is centered either just above it or just below it (depending on whether the Si atom is the one above or below a Mo atom), and one Si second-neighbor atom located 4.94 a.u. along the z axis. In the opposite direction is a Mo atom at the same distance in the experimental geometry.

In the $MoSi_2$ structure the Si atom has the position $(0,0,\pm uc)$. The variable u is a free parameter in the structure. In general, a complete calculation of the equilibrium geometry would simultaneously relax u, a, and c. However, in practice, such a complete total energy minimization would require a large computational effort. To determine the stable value of u we have instead calculated the total energy as a function of u for two different sets of a and c: (1) their experimental values, and (2) their theoretically predicted values (cf. the last set of entries in Table III). In both cases a minimum in the total energy was found for $u = \frac{1}{3}$, which suggests that this value for u is independent of a and c in our calculations (at least in a range near the experimental values for a and c). Our value for u, which is the same as the experimental value,[37] is slightly different from that given by the NC-PP calculations,[10,11] which predicted the Si atoms to be at $(0, 0, \pm 0.337c)$.

The strain tensors defined in Sec. II were used to obtain the stress tensor τ and the elastic constants C_{ij} of $MoSi_2$. The difference in the LDA total energies for each kind of strain is depicted in Fig. 8. The solid curves are least-squares fits to the data using a third-order polynomial. Note that the shift in the curves is due to the linear term. The coefficients of the fitted polynomials are compared with the linear equations given by the second and the third terms of Eq. (5) for the appropriate type of strain. The results for the stress tensor and the elastic constants are displayed in Tables IV and V, respectively. The same type of arguments given in Sec. II A for Mo can be used to show that C_{11} and C_{33} are, respectively, larger than C_{44} and C_{66}, but provide no guidance on the relative sizes of C_{44} and C_{66}. In our calculation they are almost equal. The charge-density contours in the (001) and (100) plane

suggest that the bonds between Mo and its Si nearest neighbors are stronger than between two different Mo in the (001) plane. This could explain why C_{33} is larger than C_{11}.

Because we have no experimental values to compare with, we have used the empirical formula of Fine, Brown, and Marcus[40] to check the reasonableness of our elastic constants. This formula relates the melting temperature to the elastic constants for tetragonal metals and intermetallics:

$$T_m = 354 + 4.5(2C_{11} + C_{33})/3 \,, \tag{10}$$

where T_m is in K, C_{11} and C_{33} in GPa. When our calculated elastic constants are substituted into this expression, we find a melting temperature for $MoSi_2$ of 2361 ± 6 K, which is in fairly good agreement with the measured melting temperature[41] of 2293 K.

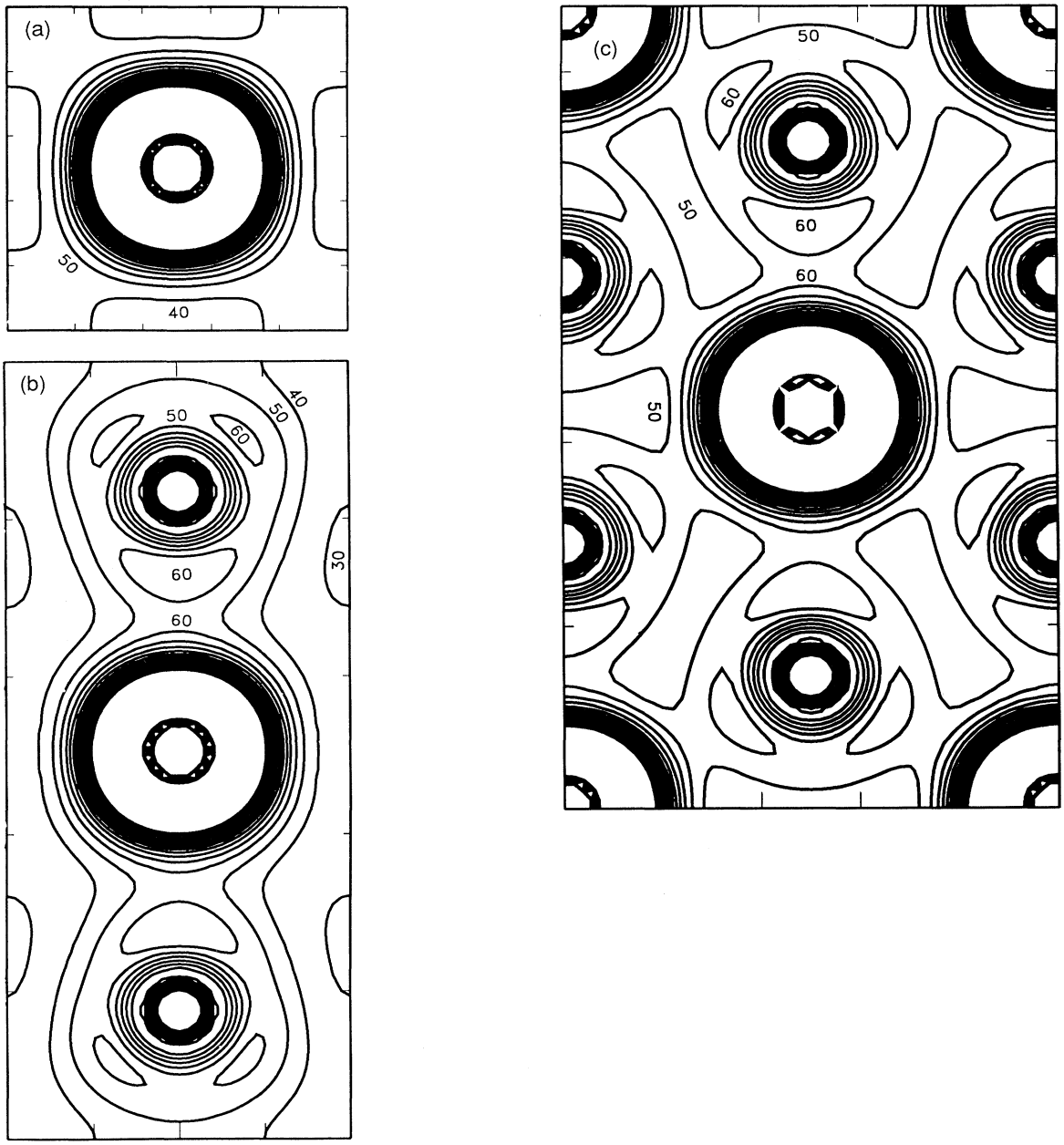

FIG. 6. Contour plots of constant charge density of $MoSi_2$, in steps of 10 millielectrons per cubic Bohr for the (a) (001) plane, (b) (100) plane, and (c) (110) plane. The larger atoms (e.g., in the center of each figure) are the Mo atoms; the smaller atoms are the Si atoms. Only the bonding regions of the charge density contours are labeled. The steps between the inner contours are also 10 millielectrons per cubic bohr.

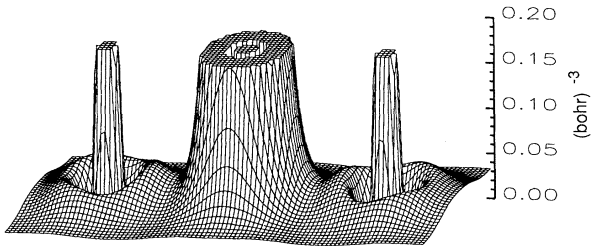

FIG. 7. Three-dimensional plot of the charge density of $MoSi_2$ in the (100) plane. The height above the plane is the charge density as a function of position in the (100) plane. The atom in the center of the figure is the Mo atom. Notice that we have cut the charge density at 0.2 electrons/bohr^3 in order to better visualize the bonding regions.

The ground-state crystalline structure of Mo and $MoSi_2$ can also be determined from the calculated stress tensor and elastic constants by minimizing the elastic energy given in Eq. (5) with respect to the strain tensor. The minimization procedure gives the following linear equations for the strain tensor:

$$\tau_i + C_{ij} e_j = 0 \ . \tag{11}$$

Because the elastic theory is only valid for small distortions (otherwise we would need to keep more terms in the expansion of the total energy as a function of strain), the solution to this equation is only valid if the predicted minimum is near the starting point, which, in our case, is the experimental structure. Using the elastic constants of Mo given in Table II and the calculated stress tensor, we have found the equilibrium lattice parameter to be 5.98 ± 0.01 a.u., which is very close to the value 5.97 ± 0.01 a.u. predicted by the total energy minimization. For $MoSi_2$, when the stress tensor and elastic constants given in Tables IV and V were used, the solution of Eq. (11) gave $a = 6.00 \pm 0.01$ a.u. and $c = 14.85 \pm 0.01$ a.u. Although the low-temperature crystalline structure of $MoSi_2$ is unknown, these values are 0.8%, and 0.1% smaller than the experimental values obtained at room temperature.[38] From Eq. (5), the total energy obtained by minimizing the elastic energy is about 0.7 mRy below that of the experimental lattice structure. By way of comparison, the ground-state total energy obtained by direct LDA calculation shows a minimum that is about 0.4 mRy lower in energy than that for the experimental structure. Overall, the differences in total energy obtained using these two different methods are near the limit which the calculations can reliably distinguish. Therefore, we conclude that the experimental geometry is consistent with the structure predicted by both methods, within the accuracy of our calculations.

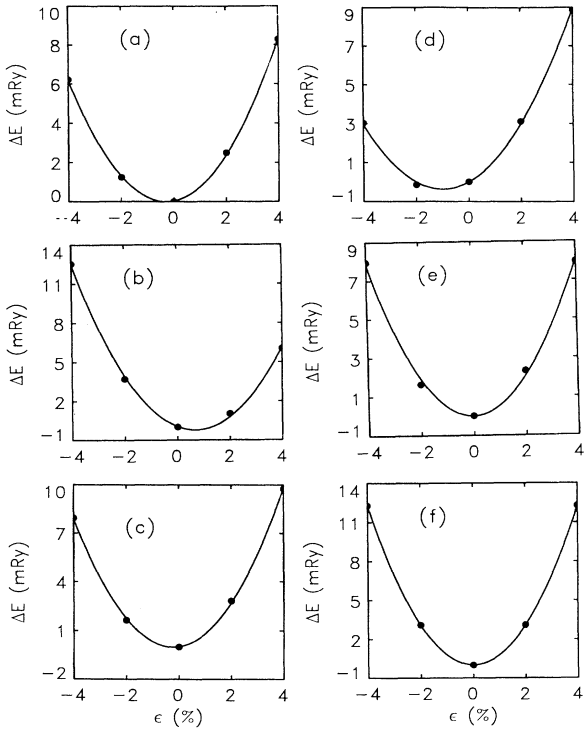

FIG. 8. Difference in total energy of $MoSi_2$ vs strain. (a)–(f) represent different kinds of strains (see text).

IV. CONCLUSION

We have used a recently developed FP-LMTO method to solve the LDA equations in order to study the structural and elastic properties of Mo and $MoSi_2$. The structural properties and the elastic constants of Mo were found to be in fairly good agreement with the experimental results. An argument using bond stretching between the nearest-neighbor atoms was given to explain qualitatively the reason for C_{11} being larger than C_{44}.

There are very few experimental results for $MoSi_2$. Most of the features present in the angle-integrated photoemission spectra have been satisfactorily explained in terms of the various peaks of our calculated DOS. We have found that the lattice constants and the cohesive energy reproduce fairly well the available experimental results.[34,37,38] However, since there have been no calculations or experimental determination of the elastic constants, our calculations for these quantities are an LDA prediction. We have tested the accuracy of these elastic constants by using them in an empirical formula to calculate the melting temperature of $MoSi_2$; good agreement with the experimental results is obtained.[41] The same ar-

TABLE IV. Calculated stress tensor τ of body-centered tetragonal $MoSi_2$ in units of mRy/a.u.^{3}.

τ_1	τ_2	τ_3	τ_4	τ_5	τ_6
0.308±0.004	0.308±0.004	0.079±0.001	0.0	0.0	0.0

TABLE V. Calculated elastic constants of body-centered tetragonal $MoSi_2$ in units of 10^{12} dyn/cm^2.

C_{11}	C_{12}	C_{13}	C_{33}	C_{44}	C_{66}
4.01±0.01	1.02±0.06	0.78±0.06	5.36±0.02	2.08±0.01	1.98±0.02

gument used for Mo involving bond stretching explains qualitatively why C_{11} and C_{33} have to be larger than C_{44} and C_{66}, in agreement with our findings. We have also explained qualitatively the reason for C_{33} being larger than C_{11} in terms of bond strength between Mo and the nearest-neighbor Si atoms and between the Mo atoms in the (001) plane.

The stress tensor and the elastic constants were also used to predict the ground-state crystalline structures for both Mo and $MoSi_2$. We have minimized the elastic energy with respect to the strain tensor and have found that the geometries of Mo and $MoSi_2$ predicted this way were fairly consistent with the structures predicted by minimizing the total energy, within the accuracy of our calculations.

ACKNOWLEDGMENTS

This work has been supported by the Energy Conversion and Utilization Technologies (ECUT) Division of the United States Department of Energy. We thank Shao-Ping Chen for providing us with some information on $MoSi_2$.

[1] K. N. Tu and J. W. Mayer, in *Thin Films—Interdiffusion and Interactions*, edited by J. M. Poate, K. N. Tu, and J. W. Mayer (Wiley, New York, 1978), p. 359.
[2] S. P. Murarka, J. Vac. Sci. Technol. **17**, 775 (1980); G. Ottaviani, *ibid.* **18**, 924 (1981); F. Mohammadi, Solid State Technol. **24**, 65 (1981).
[3] A. Franciosi, J. H. Weaver, and F. A. Schmidt, Phys. Rev. B **27**, 3554 (1983).
[4] K. N. Tu and J. W. Mayer, in *Thin Films—Interdiffusion and Reactions*, edited by J. M. Poate, K. N. Tu, and J. W. Mayer (Wiley, New York, 1980).
[5] J. H. Weaver, V. L. Moruzzi, and F. A. Schmidt, Phys. Rev. B **23** 2916 (1981).
[6] O. Bisi and L. W. Chiao, Phys. Rev. B 25, 4943 (1982), and references therein.
[7] J. H. Weaver, V. L. Moruzzi, and F. A. Schmidt, Phys. Rev. B **29**, 3293 (1984), and references therein.
[8] B. Bhattacharyya, D. M. Bylander, and L. Kleinman, Phys. Rev. B **31**, 2049 (1985).
[9] B. Bhattacharyya, D. M. Bylander, and L. Kleinman, Phys. Rev. B **31**, 5462 (1985).
[10] B. Bhattacharyya, D. M. Bylander, and L. Kleinman, Phys. Rev. B **32**, 7973 (1985).
[11] M. J. Zhu, D. M. Bylander, and L. Kleinman, Phys. Rev. B **36**, 3182 (1987).
[12] T. Shaoping and Z. Kaiming, J. Phys. C **21**, 1469 (1988)
[13] S. Tang, K. Zhang, and X. Xi, J. Phys. C **21**, L777 (1988).
[14] J. B. Berkowitz-Mattuck, M. Rossetti, and D. W. Lee, Metallurgical Trans. **1**, 479 (1970); Joan B. Berkowitz-Mattuck, Paul E. Blackburn, and Edward J. Felten, Trans. Metall. Soc. AIME **233**, 1093 (1965).
[15] V. L. Morruzzi, J. F. Janak, and A. R. Williams, *Calculated Electronic Properties of Metals* (Pergamon, New York 1978), p. 128.
[16] A. Zunger and M. L. Cohen, Phys. Rev. B **19**, 568 (1979).
[17] B. N. Harmon, W. Weber, and D. R. Hamann, J. Phys. (Paris) Colloq. **42**, CG-628 (1981).
[18] K. M. Ho, C. L. Fu, B. N. Harmon, W. Weber, and D. R. Hamann, Phys. Rev. Lett. **49**, 673 (1982).
[19] C. T. Chan, D. Vanderbilt, S. G. Louie, and J. R. Chelikowsky, Phys. Rev. B **33**, 7941 (1986).
[20] M. Dacorogna, J. Ashkenazi, and M. Peter, Phys. Rev. B **26**, 1527 (1982).
[21] L. F. Mattheiss and D. R. Hamann, Phys. Rev. B **33**, 823 (1986), and references therein.
[22] B. K. Godwal and R. Jeanloz, Phys. Rev. B **41**, 7440 (1990).
[23] N. E. Christensen (private communication).
[24] P. Hohenberg and W. Kohn, Phys. Rev. **136**, B864 (1964); W. Kohn and L. J. Sham, *ibid.* **140**, A1133 (1965).
[25] M. Methfessel, Phys. Rev. B **38**, 1537 (1988).
[26] M. Methfessel, C. O. Rodriguez, and O. K. Andersen, Phys. Rev. B **40**, 2009 (1989).
[27] A. T. Paxton, M. Methfessel, and H. M. Polatoglou, Phys. Rev. B **41**, 8127 (1990).
[28] O. K. Andersen, Phys. Rev. B **12**, 3012 (1975).
[29] D. J. Chadi and M. L. Cohen, Phys. Rev. B **8**, 5747 (1973).
[30] U. Von Barth and L. Hedin, J. Phys. C **5**, 1629 (1988).
[31] C. L. Fu and K. M. Ho, Phys. Rev. B **28**, 5480 (1983).
[32] D. C. Wallace, *Thermodynamics of Crystals* (Wiley, New York, 1972).
[33] J. Birch, J. Geophys. Res. **83**, 1257 (1978).
[34] C. Kittel, *Introduction to Solid State Physics*, 5th ed. (Wiley, New York, 1976)
[35] K. W. Katahara, M. H. Manghnani, and E. S. Fisher, J. Phys. F **9**, 773 (1979).
[36] F. H. Featherstone and J. R. Neighbours, Phys. Rev. **130**, 1324 (1963).
[37] H. J. Goldschmidt, *Interstitial Compounds* (Plenum, New York, 1967).
[38] *Metallography, Structures and Phase Diagrams* (American Society for Metals, Metals Park, Ohio, 1973), Vol. 8, p. 237.
[39] The experimental cohesive energy is calculated using the heat of formation of $MoSi_2$ from Ref. 37, and the cohesive energies of Mo and Si from Ref. 33. Note that $E_{\rm coh}^{\rm MoSi_2} = H_f^{\rm MoSi_2} + E_{\rm coh}^{\rm Mo} + 2E_{\rm coh}^{\rm Si}$.
[40] M. E. Fine, L. D. Brown, and H. L. Marcus, Scr. Metall. **18**, 951 (1984).
[41] *Binary Alloy Phase Diagrams*, edited by T. B. Massalski (American Society for Metals, Metals Park, Ohio, 1986), p. 1631.